Bioactive Materials 5 (2020) 611–623

Contents lists available at ScienceDirect

Bioactive Materials

journal homepage: http://www.keaipublishing.com/biomat

Layer-by-layer deposition of bioactive layers on magnesium alloy stent materials to improve corrosion resistance and biocompatibility

Fan Gao[a,1], Youdong Hu[b,1], Guicai Li[c], Sen Liu[a], Li Quan[a], Zhongmei Yang[a], Yanchun Wei[a], Changjiang Pan[a,*]

[a] Faculty of Mechanical and Material Engineering, Huaiyin Institute of Technology, Huai'an 223003, China
[b] Department of Geriatrics, The Affiliated Huai'an Hospital of Xuzhou Medical University, Huai'an 223003, China
[c] Jiangsu Key Laboratory of Nerve Regeneration, Nantong University, Nantong 226001, China

ARTICLE INFO

Keywords:
Magnesium alloys
Graphene oxide
Heparin
Corrosion resistance
Blood compatibility
Endothelial cells

ABSTRACT

Magnesium alloy is considered as one of the ideal cardiovascular stent materials owing to its good mechanical properties and biodegradability. However, the *in vivo* rapid degradation rate and the insufficient biocompatibility restrict its clinical applications. In this study, the magnesium alloy (AZ31B) was modified by combining the surface chemical treatment and in-situ self-assembly of 16-phosphonyl-hexadecanoic acid, followed by the immobilization of chitosan-functionalized graphene oxide (GOCS). Heparin (Hep) and GOCS were alternatively immobilized on the GOCS-modified surface through layer by layer (LBL) to construct the GOCS/Hep bioactive multilayer coating, and the corrosion resistance and biocompatibility were extensively explored. The results showed that the GOCS/Hep bioactive multilayer coating can endow magnesium alloys with an excellent *in vitro* corrosion resistance. The GOCS/Hep multilayer coating can significantly reduce the hemolysis rate and the platelet adhesion and activation, resulting in an excellent blood compatibility. In addition, the multilayer coating can not only enhance the adhesion and proliferation of the endothelial cells, but also promote the vascular endothelial growth factor (VEGF) and nitric oxide (NO) expression of the attached endothelial cells on the surfaces. Therefore, the method of the present study can be used to simultaneously control the corrosion resistance and improve the biocompatibility of the magnesium alloys, which is expected to promote the application of magnesium alloys in biomaterials or medical devices, especially cardiovascular stent.

1. Introduction

Cardiovascular disease is a global disease with high mortality and its incidence has been increasing continuously. After drug therapy and surgical treatment (such as coronary artery bypass grafting), interventional therapy, represented by stent insertion, has become the main effective method to treat the stenotic cardiovascular disease. However, severe inflammatory reactions and high in-stent restenosis (ISR) rate (20–30%) occur frequently after the implantation of bare metal stents, leading to higher mortality [1]. Although the drug-eluting stent can release anti-proliferative drugs loaded on the stent surface to significantly reduce the ISR incidence, the released drugs (such as rapamycin and paclitaxel) can also inhibit the endothelium healing when it prevents the smooth muscle cells proliferation. Therefore, it may delay the regeneration of natural vascular intima and increase the risk of subacute thrombosis, late thrombosis and in-stent restenosis [2].

In recent years, the third-generation biodegradable vascular stent has been widely concerned. After vascular remodeling, the biodegradable stent can be safely adsorbed by human body. The degradation products are excreted from the body through metabolism without restenosis, thrombosis and other complications, consequently, it may completely solve the clinical problems of the bare metal stent and drug-eluting stent. Magnesium and its alloys are one kind of the ideal candidates to prepare the biodegradable vascular stents because of their suitable mechanical properties and the non-toxic degradation products [3,4]. However, magnesium alloy degrades fast *in vivo* due to its active chemical properties under the physiological conditions. Upon degradation, it is easy to produce excessive hydrogen gas, increase the local alkalinity and enrich the secondary corrosion products around the implanted tissue, resulting in the premature loss of the mechanical

Peer review under responsibility of KeAi Communications Co., Ltd.
* Corresponding author.
E-mail address: panchangjiang@hyit.edu.cn (C. Pan).
[1] These authors contributed equally to this work and should be considered co-first authors.

https://doi.org/10.1016/j.bioactmat.2020.04.016
Received 14 March 2020; Received in revised form 20 April 2020; Accepted 22 April 2020

properties and the limited biocompatibility. The toxic reaction to the surrounding tissue can delay the intima tissue healing and regeneration and eventually lead to the implantation failure. It is well known that the corrosion resistance and biocompatibility of the magnesium alloys are closely associated with the surface properties, therefore, surface modification represents an effective approach to control the electrochemical corrosion behavior and improve the blood compatibility, as well as promote the endothelial tissue healing.

Basically, two main strategies, including alloying and surface modification, are usually applied to enhance the corrosion resistance of the magnesium alloys. The corrosion resistance of the magnesium alloys is affected by many factors such as metallographic structure and impurities, therefore reducing the content of harmful impurity elements such as Co, Ni, Ba, Cd and adding some beneficial alloy elements (including Ca, Mn, Y, RE, Zn, Sn, Sr, Zr, Al, etc) can refine the grains and strengthen the second phase, as well as reduce the cracking of the passivation film, finally leading to the improved corrosion resistance, excellent mechanical properties and better biocompatibility to some degree [5,6]. Surface modification is another effective, facile, and popular way to improve the corrosion resistance and biocompatibility. The current surface modification methods mainly consist of three strategies, including the formation of the chemical conversion layer by chemical treatment or electrochemical treatment (such as micro arc oxidation, fluorination treatment, alkali heat treatment.), construction of the surface modified layer by plasma treatment and ion implantation, and deposition of the inorganic coating or introduction of the organic bioactive molecules to form the surface covering coating (such as hydroxyapatite, self-assembly layer and polymer coating.) [7,8]. Although a plenty of works regarding surface modification of the magnesium alloys has been reported [9–11], the current methods have not achieved the satisfactory clinical results. As a biodegradable stent material, there are still many problems, including endothelium hyperplasia, thrombosis and stent collapse caused by the fast corrosion, to be solved [12].

Magnesium alloys, as a vascular stent material, should have the controllable biodegradability and excellent biocompatibility, as well as the abilities to regulate the physiological responses of human blood and surrounding environment [13,14]. Layer by layer (LBL) is a novel and facile surface modification technology which is based on the electrostatic interaction of the electrolytes with opposite charges. It has been widely used for surface modification of biomaterials to improve the biocompatibility [15]. It can also be used to modify the magnesium alloy surface to introduce a variety of bioactive molecules to build a bioactive surface with specific functions so that the modified surface can effectively regulate the interfacial interactions between the implant and surrounding environment [16]. Simultaneously, the multilayer structure can effectively increase the amount of the biomolecules and increase the coating thickness to control the *in vitro* and *in vivo* electrochemical degradation behaviors and biocompatibility.

Graphene oxide (GO) is a nanomaterial with a single-carbon structure, and it has a huge specific surface area, good mechanical properties and biocompatibility. The oxygen-containing groups (including carboxyl, hydroxyl and epoxy groups.) on GO surface can effectively enhance the corrosion resistance of the magnesium alloy when it is deposited on the magnesium alloy surface [17]. At the same time, GO can promote cell adhesion and proliferation due to its ability to adsorb extracellular matrix proteins by noncovalent interactions, electrostatic forces or hydrogen bond. In addition, the active groups of GO can be linked with other biomolecules to enhance its bioactivities [18,19]. Chitosan is a kind of natural derived polysaccharide polymer with good biocompatibility and biodegradability, it can promote cell adhesion and proliferation. At the same time, chitosan contains a lot of positive charges and has good antibacterial properties [20,21]. Therefore, functionalization of GO by chitosan can significantly enhance its biocompatibility, and the immobilization of chitosan-functionalized GO on the magnesium alloy surface can not only enhance the corrosion resistance, but also obtain a better bioactivity. In addition, the chitosan-functionalized GO coating can create a positive charged surface to bind the negatively charged biomolecules. Heparin is a kind of polysaccharide with negative charges and excellent anticoagulant, and it is widely used in the surface modification of biomaterials to improve the blood compatibility. Heparin combined with related drugs can inhibit the formation of inflammation [22] and promote the endothelial cell growth to a certain extent [23]. The strong electronegativity of heparin endows it with better ability to bind with the positively charged substances to fabricate the bioactive multilayer coating.

In view of the limited corrosion resistance and poor biocompatibility of the magnesium alloys, in the present study, graphene oxide (GO) was firstly functionalized by chitosan to prepare chitosan-functionalized GO (GOCS), and then GOCS was grafted on the AZ31B magnesium alloy surface. Finally, negative charged heparin and positive charged GOCS were alternatively deposited on the GOCS-functionalized magnesium alloy to prepare the GOCS/Hep multilayer bioactive coating. The advantage of the multilayer coating is that it cannot only improve the corrosion resistance of the magnesium alloy, but also endow the surface with good blood compatibility as well as promote the adhesion and proliferation of the endothelial cells, thus the multifunctional surface can be obtained.

2. Materials and methods

2.1. Surface modification of magnesium alloy

The chitosan-functionalized GO was firstly prepared. To this end, GO (XFNANO Materials Tech Co., Ltd, Nanjing, China. The GO thickness and diameter are about 0.8–1.2 nm and 0.5–5 μm, respectively.) was fully dispersed ultrasonically in the deionized water to obtain a 1 mg/ml dispersion, and chitosan (Adamas Reagent Co., Ltd) was dissolved into 0.2% acetic acid (pH = 5) to form a 5 mg/ml solution. The solutions of graphene oxide and chitosan were thoroughly mixed according to the volume ratio of 1:5, and then 10 mM EDC/NHS (3:1) was added. After magnetic stirring for 12 h, the solution was put into the dialysis bag (MW: 3500) in the deionized water for 5 days to obtain the chitosan-functionalized graphene oxide (GOCS).

The AZ31B magnesium alloy sheet (15 mm diameter, 3 mm thickness) was successively polished by the 400#, 600#, 800#, 1200#, 2000# sandpapers. After ultrasonically cleaned with acetone, deionized water and anhydrous ethanol for 10 min, respectively, the sample was put into a 3 M 75 °C NaOH solution to treat 24 h and it was recorded as Mg–OH. After cleaned and dried by the compressed air, Mg–OH sample was modified by immersing it into 5 mM 16-phosphonyl-hexadecanoic acid solution (in ethanol) for 24 h. The sample was then treated at 120 °C in an oven for 12 h and recorded as Mg-16. Mg-16 was immersed into EDC/NHS solution (10 mM) for 2 h to activate the surface, followed by incubating 2 h in GOCS solution (6 mg/ml) to fabricate GOCS-modified surface, and the obtained sample was recorded as Mg-GOCS. Finally, the Mg-GOCS was alternatively immersed into heparin solution (2 mg/ml) and GOCS solution for 20 min each time. One circle of deposition of GOCS and heparin is defined as one layer, and five layers, i.e., Mg-GOCS/He/$(GOCS/Hep)_4$, were fabricated. The outermost layer is heparin and the final sample was recorded as Mg-GOCS/Hep.

2.2. Surface characterization

The attenuated total reflection Fourier transform infrared spectrum (ATR-FTIR, TENSOR 27, Bruker of Germany) was done to characterize the chemical structures of the pristine and modified surfaces. The measurement was carried out at room temperature, and the scanning range was 4000 cm^{-1}-650 cm^{-1}. The graphene oxide coating was analyzed by Raman spectroscopy (Renishaw, UK, RM 2000). Scanning electron microscopy (SEM, FEI Quata 250, USA) was used to observe the surface morphologies, and energy dispersive X-Ray Spectroscopy (EDS, IMA X-MAX 20, Britain) was carried out to scan the surface to

Table 1
The concentration of composition in SBF.

Reagent	NaCl	KCl	$NaHCO_3$	$CaCl_2$	Na_2HPO_4	KH_2PO_4	$MgSO_4$	Glucose
Concentration (g/L)	8	0.4	0.35	0.14	0.06	0.06	0.01	1

determine the composition of the surface elements.

2.3. Electrochemical and corrosion behaviors

2.3.1. Potentiodynamic polarization curves and EIS

The potentiodynamic polarization curves of the modified and pristine magnesium alloys in SBF were plotted on a Chi660D electrochemical workstation (CHI Instruments, Inc., Shanghai, China) using the standard three electrode system (sample as the working electrode, platinum wire as the auxiliary electrode, Ag/AgCl as the reference electrode). The samples were immersed in the simulated body fluid (SBF, the composition is shown in Table 1.) for 10min until the corrosion potential was stable before testing, the scan scope was from - 2V to - 1V and the scanning speed was 1 mV/s. Tafel extrapolation method was used to fit the corrosion potential and corrosion current density, and the annual corrosion depth was determined based on equation (1):

$$d = 3.28 \times 10^{-3} (M/n\rho) I_{corr} \quad (1)$$

Where d is the annual corrosion depth (mm/y), M is the atomic weight of Mg (24.3 g/mol), n is the atomic valence of Mg (n = 2), ρ is the density of Mg (1.78 g/cm^3), I_{corr} is the corrosion current density (μA.cm^{-2}).

The Chi660D electrochemical workstation was also used to record the electrochemical impedance spectroscopy (EIS). The scanning frequency was from 10^5 Hz to 0.1 Hz. The disturbance signal was a sinusoidal alternating current potential with an amplitude of 10 mV. The sample was soaked in SBF for 10 min for a stable open circuit potential before testing.

2.3.2. Corrosion microtopography

The samples were firstly sealed with the silicone rubber, only exposing the modified surface (1.77 cm^2). The samples were immersed into 20 ml SBF solution at 37 °C for 1 d, 3 d and 7 d, respectively, and the SBF was changed every 2 days. After the immersion, the surface was cleaned by the deionized water, dried in an oven, and then the corrosion morphologies were observed by SEM (FEI Quata 250, USA).

2.3.3. pH changes

The sample was sealed with the silicone rubber to expose the testing area (1.77 cm^2), and then soaked in 20 ml SBF solution and kept at 37 °C. The pH values of the solutions were measured by a pH meter at the predetermined time. Three parallel samples were measured and the average value was obtained. Finally, the pH value change curves were plotted.

2.3.4. Mg^{2+} release

The sealed magnesium alloys (the exposed area was 1.77 cm^2) were immersed into 20 ml 37 °C SBF solution. The solution was collected at the predetermined time and compensated for the same amount of the fresh solution. Then the concentration of Mg^{2+} was measured by an inductively coupled plasma emission spectrometer (Optima 7000 DV), and the release profile of Mg^{2+} was obtained according to the standard curve.

2.4. Blood compatibility

2.4.1. Platelet adhesion

Firstly, the platelet-rich plasma (PRP) was obtained by centrifuging the anticoagulant human whole blood from a healthy volunteer for 15 min at 1500 r/min. 100 μl PRP was covered onto the sample surface, cultured in a 37 °C incubator for 2 h, washed twice with normal saline, and then fixed 1.5 h with 2.5% glutaraldehyde solution. Finally, the adhered platelets were successively dehydrated with 50%, 70%, 90%, and 100% anhydrous ethanol. After drying, the number and morphologies of the platelets attached on the sample surface were observed by SEM. 10 platelet images with small magnification were randomly selected from each sample for counting the number of platelets, and the data was expressed as platelets per unit area.

2.4.2. cGMP assay

Firstly, 100 μl platelet rich plasma was dropped on the sample surface to incubate 1 h at 37 °C. The cGMP (guanosine cyclophosphate) concentration was determined by cGMP ELISA kit. In brief, a series of standard solutions with the concentrations of 12 nm/L, 6 nm/L, 3 nm/L, 1.5 nm/L and 0.75 nm/L were prepared. The standard solutions and 40 μl sample diluent were added into the standard hole and the sample hole, respectively. Subsequently, 10 μl PRP plasma was added for each hole and the plate was incubated at 37 °C for 30min. The liquid was suck out and the plate was washed 5 times, 50 μl enzyme standard reagent was added to incubate another 30 min. The chromogenic agent A and B were added in turn and kept in the dark environment at 37 °C for 10min. Finally, the termination solution was added and the absorbance was measured at 450 nm cGMP value was determined by the standard curve.

2.4.3. Hemolysis rate

The fresh anticoagulant whole blood was collected from a healthy volunteer and then centrifuged at 1500 r/min for 15min. The red blood cells were prepared into 2% red blood cell dispersion with normal saline. The sample was immersed into 2 ml red blood cell solution and cultured 3 h at 37 °C. Subsequently, 1 ml red blood cell solution was centrifuged and the absorbance of supernatant was measured at 450 nm using a Microplate Reader (Bio-Tek, Eons). A 2% red blood cell solution with the distilled water was used as the positive control, and the 2% red blood cell solution with normal saline was used as the negative control. The hemolysis rate was calculated by equation (2):

$$\text{Hemolysis}(\%) = (\text{ODs-ODn})/(\text{ODp-ODn}) \times 100\% \quad (2)$$

Where OD_s is the absorbance value of the sample, OD_n is the negative control value, and OD_p is the positive control value.

2.5. Endothelial cell behaviors

2.5.1. Endothelial cell adhesion

The samples were placed in a 24-well culture plate and then irradiated by the ultraviolet light for one night. The samples were washed twice by the aseptic physiological saline. Each sample surface was added with 1.5 ml culture medium (DMEM F12 containing 5% FBS and 1% Penicillin Streptomycin) and 0.5 ml endothelial cells (5×10^4 cells/ml). The samples were incubated at 37 °C with 5% CO_2 for 1 d and 3 d, respectively. After removing the culture medium, the sample was washed twice with the physiological saline, and the cells were fixed by 2.5% glutaraldehyde at 4 °C for 1.5 h. The attached cells were stained with 10 μg/ml rhodamine (in PBS) and 500 ng/ml DAPI (in ultrapure water), respectively. The fluorescent images were taken by a fluorescent microscopy (Zeiss, inverted A2).

2.5.2. Endothelial cells proliferation

CCK-8 assay was used to determine the proliferation behaviors of the endothelial cells. The sample was placed into the culture plate, and then 1.5 ml cell culture medium and 0.5 ml endothelial cells were added into each well (5×10^4 cells/ml) to incubate 1 d and 3 d at 37 °C with 5% CO_2, respectively. 0.5 ml 10% CCK-8 solution (in DMEM F12) was added into the plate well to culture 3.5 h. Subsequently, 200 μl CKK-8 solution was added and the absorbance at 450 nm was measured. Three parallel samples were measured and the average value was calculated.

2.5.3. VEGF expression

The cells were inoculated on the sample surface (5×10^4 cells/ml) to incubate for 1 d and 3 d at 37 °C, respectively. The concentration of VEGF in the cell culture medium was measured by a VEGF ELISA kit. In brief, the standard solutions with the concentrations of 320 ng/L, 160 ng/L, 80 ng/L, 40 ng/L and 20 ng/L were prepared and added to the standard hole. 40 μl sample diluent and 10 μl cell culture solution were added to the sample hole to incubate 30 min. After washed 5 times, 50 μl enzyme standard reagent was added and then incubated and washed again. 50 μl chromogenic reagent A and 50 μl chromogenic reagent B were added and placed at 37 °C for 10min. Finally, 50 μl termination solution was added to the hole, the absorbance (OD value) was measured at 450 nm, and the VEGF concentration in the sample hole was calculated according to the standard curve.

2.5.4. NO release

The endothelial cells were cultured on the sample surface for 1 d and 3 d, respectively. The NO concentration in the culture medium was determined by the nitrate reductase method. The standard solutions with the concentrations of 0 μM/L, 1 μM/L, 2 μM/L, 5 μM/L, 10 μM/L, 20 μM/L, 40 μM/L, 60 μM/L and 100 μM/L were prepared with DMEM F12 cell culture medium containing 10% FBS. The supernatant of 50 μl cell culture medium was added to the sample hole, then 50 μl Griess Reagent I and 50 μl Griess Reagent II were added in turn. Finally, the absorbance at 540 nm was measured. The NO concentration was calculated according to the standard curve.

3. Results and discussion

3.1. Surface characterization

The chemical properties of the magnesium alloys are very active and the *in vivo* corrosion rate is over-fast. The construction of the different functional coatings on the surface to isolate the magnesium alloy substrate from the corrosion medium represents an important and effective approach to enhance the corrosion resistance. In this study, the GOCS/Hep multilayer coating was constructed by LBL to regulate the corrosion electrochemical behaviors and enhance the biocompatibility. ATR-FTIR was firstly used to characterize the functional groups of the pristine and modified magnesium alloys, and the results are shown in Fig. 1(a). Clearly, almost no infrared absorption can be detected on the blank magnesium surface. The strong absorption peak at 3700 cm^{-1} on Mg–OH indicated that alkali heat treatment can produce a large amount of –OH on the surface. These hydroxyls can not only provide reaction sites for the self-assembly of 16-phosphonyl- hexadecanoic acid, but also significantly improve the hydrophilicity. At the same time, the appearance of the hydroxyl groups suggested that an oxide layer was produced on the surface after NaOH treatment. The oxide layer was dense and it can prevent the corrosive medium penetrating the magnesium matrix, and thus improve the corrosion resistance and biocompatibility to some degree. 16-phosphonyl hexadecanoic acid is a popular molecule for the self-assembly surface modification, in which the phosphonyl group can be immobilized on the surface by the dehydration reaction with –OH. On the other side, it can simultaneously produce a partial phosphating effect on the surface, which may be helpful to enhance the corrosion resistance. The terminal groups (-COOH) can further react with other groups such as –OH and NH_2 to introduce other bioactive substances to enhance the biocompatibility. After the immobilization of 16-phosphonyl hexadecanoic acid, the absorption peaks at 2850 cm^{-1} and 2920 cm^{-1} can be found, which can be attributed to the adsorption of $–CH_3$ and $–CH_2$, respectively. The peak at 1710 cm^{-1} belonged to the adsorption of C═O in the carboxyl group. These results demonstrated that 16-phosphonyl-hexadecanoic acid was successfully immobilized on Mg–OH surface, and a carboxyl modified surface was also obtained successfully. The carboxyl on the surface can be linked with $–NH_2$ of chitosan. Therefore, after further immobilization of GOCS on the surface, the infrared absorption peak of the carbonyl group in the amide appeared at 1680 cm^{-1}. The absorption peaks of N–H and C–N can be observed at 1600 cm^{-1} and 1425 cm^{-1}, respectively, indicating that GOCS was successfully grafted on the surface. Heparin contains many sulfonic acid groups and carboxyl groups. These groups make heparin exhibiting negatively charged characteristics and thus heparin can electrostatically adsorb with the positively charged GOCS. After electrostatic adsorption of heparin on the surface, the infrared absorption of the sulfonic acid group at 1038 cm^{-1} and C═O around 1710 cm^{-1} can be detected, suggesting that heparin was successfully introduced on the surface.

The GO structure on the surface was further characterized by Raman spectroscopy. Because there was no Raman adsorption of Mg, Mg–OH and Mg-16, the blank Mg was used as a reference, and Fig. 1(b) shows the Raman spectra of Mg and Mg-GOCS/Hep. The Raman spectrum of Mg surface was almost a straight line without Raman absorption, while the surface of Mg-GOCS/Hep had G peak around 1590 cm^{-1} and D peak at 1350 cm^{-1}, which are the characteristic peaks of graphene oxide [24]. The G peak was caused by the in-plane vibration of sp^2 carbon atoms and represented an ordered hybrid sp^2 carbon atom. The presence of D peak indicated that there had been disordered hybrid sp^3 carbon atoms in graphene oxide. The higher the D peak was, the more sp^3 carbon atoms were present. The D peak was a disordered vibrational peak, which indicated that the C═C in graphene oxide was destroyed and part of the ordered sp^2 hybrid carbon atoms were transformed into sp^3 hybrid structure. Generally, the ratio of I_G/I_D represents the ratio of sp^2 and sp^3 carbon atoms and its value can be used to determine the degree of the structural defect. It can be obtained from Fig. 1(b) that the value of I_G/I_D was about 19/18, indicating that there was half of the disordered hybrid carbon atoms in graphene oxide on the Mg-GOCS/Hep surface.

With the aim of investigating the surface morphologies and surface element changes of the magnesium alloy surface, the samples were further analyzed by scanning electron microscopy (SEM) and energy dispersive X-Ray spectroscopy (EDS). The results are shown in Fig. 2 and Table 2. It can be clearly seen that the blank magnesium alloy surface was relatively smooth, and only a few scratches can be observed, the surface elements were almost Mg. However, 7.9% of O was introduced after polishing due to the surface oxidation. After alkali heat treatment, a $Mg(OH)_2$ layer was produced on the surface, leading to the obvious increase of oxygen element and the decrease of Mg and Al, but the micro morphology did not change obviously. The Mg content on Mg-16 surface decreased significantly, and C and P appeared concurrently for the first time, suggesting that 16-phosphonyl-hexadecanoic acid was successfully immobilized on the surface. After the immobilization of GOCS, the obvious granular structure of chitosan [25] can be observed and a dense protective layer, as shown in Fig. 2d, was also created. In addition, the C content increased sharply from 19.41% of Mg-16 to 35.37% of Mg-GOCS, and 7.43% of N was also detected, further indicating that GOCS was successfully grafted on the Mg-16 surface. For Mg-GOCS/Hep, the appearance of S and Na elements demonstrated that heparin had been loaded on the surface. The surface of Mg-GOCS/Hep was relatively smooth, and the Mg element dropped sharply from 24.23% of Mg-GOCS to 6.51%, indicating that the multilayer coating can cover the magnesium alloy. It can be seen

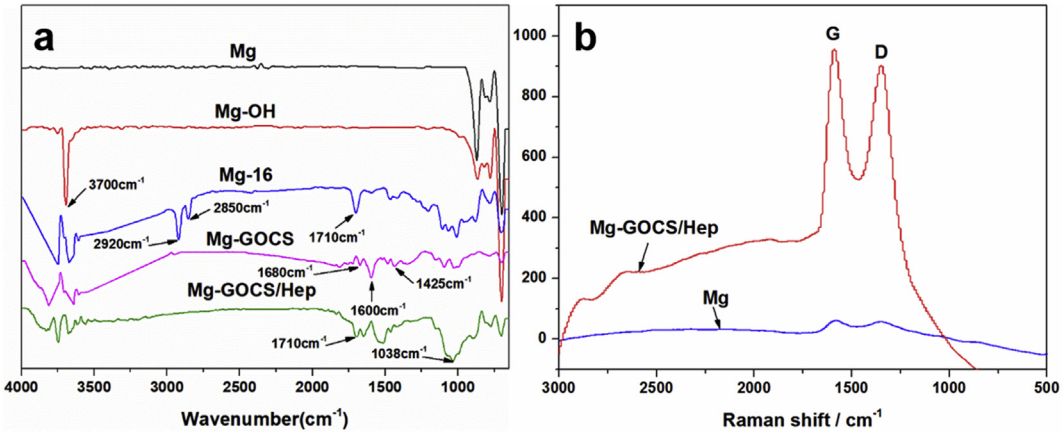

Fig. 1. ATR-FTIR (a) and Raman (b) diagram of the different samples.

from Fig. 2(f) that after five circles of deposition of GOCS and Hep, the thickness of the coating was about 7.24 μm.

3.2. Electrochemical corrosion behaviors

R_s: solution resistance; Q_1: double layer capacitive constant phase element; R_1: charge transfer resistance; Q_2: coating constant phase element; R_2: coating resistance; R_p: polarization resistance; $n_1$and n_2: correlation coefficient.

Potentiodynamic polarization curve is an effective and popular method to evaluate the corrosion resistance of biomaterials. Normally, the larger natural corrosion potential represents the smaller the corrosion tendency, and the small corrosion current density means the slower corrosion rate [26]. Fig. 3a shows the potentiodynamic polarization curves of the different samples, the corresponding corrosion potential and corrosion current density as well as annual corrosion depth are shown in Table 3. It can be clearly seen that the corrosion potential of Mg was the smallest while the corrosion current density was the largest among all samples because it was easier to be corroded in SBF. The annual corrosion depth reached 2 mm/y for Mg, suggesting that the corrosion resistance of the magnesium alloy was limited and need to be improved. The over-fast corrosion made the magnesium alloy existing in the body for too short time so that it cannot play an effective supporting effect in the expected time when it was used as the cardiovascular stent materials. For Mg–OH, the corrosion potential increased by 0.242V, and the corrosion current density decreased to 2.067×10^{-5} A cm^{-2}, indicating that the corrosion resistance was significantly enhanced as compared to Mg. The annual corrosion depth (0.47 mm/y) of Mg–OH was significantly lower than that of Mg. It can be considered that the compact and dense $Mg(OH)_2$ protective layer produced by NaOH treatment can improve the corrosion resistance of the magnesium alloy. In addition, the oxide layer was also conducive to the subsequent self-assembly surface modification due to the existence of hydroxyls [27]. The immobilization of 16-phosphonyl-hexadecanoic acid not only increased the corrosion potential, but also reduced the corrosion current density and annual corrosion depth. It was considered that 16-phosphonyl-hexadecanoic acid molecule was firmly immobilized on Mg–OH surface at 120 °C, which further hindered the corrosion of Cl^- and other anions. When GOCS was covalently immobilized on the magnesium alloy surface, the corrosion potential was higher and the corrosion current density was further reduced. The annual corrosion depth was 0.2 mm/y which was only one tenth of Mg. It was convinced that graphene oxide was an inert material with a huge specific surface area and the good anti permeability to the molecules and ions in the corrosion medium [28]. GOCS can form a dense layer on the surface to inhibit the corrosion of the magnesium alloy by inorganic anions. The corrosion potential of Mg-GOCS/Hep was −1.385 V, the corrosion current density was only 1.359×10^{-6} A cm^{-2}, and the

Table 2
Elemental compositions of the different samples.

Samples	Atomic concentration (at. %)							
	Mg	O	Al	C	P	N	S	Na
Mg	89.5	7.9	2.6	–	–	–	–	–
Mg–OH	72.94	26.6	1.0	–	–	–	–	–
Mg-16	53.71	26.53	–	19.41	0.35	–	–	–
Mg-GOCS	24.23	32.97	–	35.37	–	7.43	–	–
Mg-GOCS/Hep	6.51	34.23	–	45.99	–	12.33	0.49	0.45

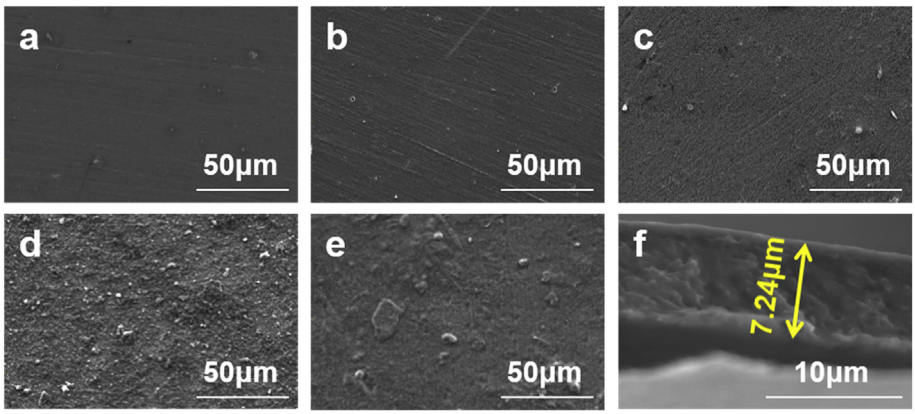

Fig. 2. Typical SEM images of Mg (a), Mg–OH (b), Mg-16 (c), Mg-GOCS (d), and Mg-GOCS/Hep (e). Image f shows the cross-section of GOCS/Hep coating.

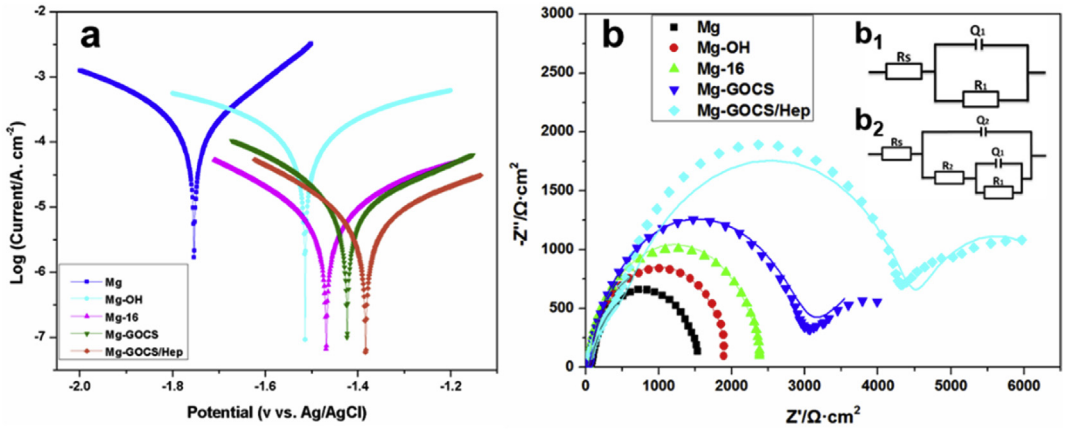

Fig. 3. (a) Potentiodynamic polarization curves of the different samples; (b) Nyquist spectroscopy diagrams of the different samples; Scatter: original values; Line: calculative values; (b_1) Equivalent circuits of Mg, Mg–OH and Mg-16; (b_2) Equivalent circuits of Mg-GOCS and Mg-GOCS/Hep.

Table 3
Corrosion potential, corrosion current density and the corrosion depth per year of the different samples.

Samples	E_{corr}/V	I_{corr}/A·cm^{-2}	d/(mm/y)
Mg	−1.755	8.841×10^{-5}	2.00
Mg–OH	−1.513	2.067×10^{-5}	0.47
Mg-16	−1.467	9.785×10^{-6}	0.22
Mg-GOCS	−1.424	8.621×10^{-6}	0.20
Mg-GOCS/Hep	−1.385	1.359×10^{-6}	0.03

annual corrosion depth was also reduced to 0.03 mm/y. After 5 cycles deposition of GOCS and heparin, a thick bioactive coating was formed on the magnesium alloy surface, which can effectively prevent aggressive ions penetrating the matrix surface, leading to excellent corrosion resistance. At the same time, the electrostatic repulsion between the negative charged heparin and the corrosive anions was one of the important factors to improve the corrosion resistance.

Electrochemical impedance spectroscopy (EIS) is another important method to explore the electrochemical behavior of biomaterials. The most widely used analytical method is to build an equivalent circuit model to fit and interpret EIS data [29]. As shown in Fig. 3b, it was obvious that only one high frequency capacitor ring can be obtained on Mg, Mg–OH and Mg-16 samples, which can be attributed to the impedance response between the surface corrosion products and the charge transfer resistance. At the same time, the capacitance rings of the modified magnesium alloys were larger than that of Mg, indicating that the corrosion resistance was improved [30]. On the EIS spectra of Mg-GOCS and Mg-GOCS/Hep, the larger high frequency capacitor ring can be attributed to the impedance of the interface reaction between the coating and the corrosion products on the surface, and it suggested that the corrosion resistance of magnesium alloy had been further enhanced. The new low frequency capacitor ring was believed to be formed by the corrosion on the magnesium alloy surface [31].

In order to describe the response of EIS spectra quantitatively, the corresponding equivalent circuit diagrams were constructed. Fig. 4b_1 is the R (QR) equivalent circuit diagram, which was used to characterize the impedance spectra of Mg, Mg–OH and Mg-16. Fig. 4b_2 is the R (Q (R (QR))) equivalent circuit diagram and it was used to analyze the impedance spectra of Mg-GOCS and Mg-GOCS/Hep. The results of EIS were fitted with the equivalent circuit diagram, and the fitting parameters are shown in Table 4. The charge transfer resistance (R_1) and coating resistance (R_2) were fitted by Zview software, and the polarization resistance (R_p) is equal to the sum of R_1 and R_2. All samples were tested in SBF; therefore, the R_S value was hardly changed. Q_1 and Q_2 represent the capacitance of the constant phase element. If n_1 and n_2 are close to 1, it means that the constant phase element is close to the pure capacitance. It was noteworthy that the capacitance of Mg-GOCS/Hep was much smaller than that of Mg-GOCS, indicating that the GOCS/Hep multilayer was more uniform and denser, which was contributed to reduce the exposure degree of the magnesium alloy surface in the corrosion medium and thus the multilayer bioactive coating can effectively improve the corrosion resistance. The polarization resistance (R_p) is an important parameter to evaluate the overall corrosion resistance of the magnesium alloy. It can be seen from Table 4 that the polarization resistance of untreated magnesium alloy was only 1482 Ω cm^2, whereas the R_p values of the modified magnesium alloys were significantly increased. The polarization impedance of Mg-GOCS/Hep was 4525 Ω cm^2, demonstrating that the multilayer coating can effectively improve the corrosion resistance of the magnesium alloys.

In order to intuitively observe the surface corrosion, the different modified magnesium alloys were soaked in SBF for 1d, 3d and 7d, respectively. The changes of the surface corrosion morphologies were observed by scanning electron microscopy, and the results are shown in Fig. 4. Obvious corrosion cracks can be observed on the unmodified magnesium alloy surface after one day, and the corrosion products accumulated after three days immersion, indicating that the corrosion rate of Mg was fast from 1d to 3d. The difference between the corrosion morphologies of 7 d and 3 d was not significant, it was considered that the accumulation of the corrosion products could isolate the magnesium surface from the corrosive medium and make the degradation rate of the magnesium alloy tend to be moderate to some degree. The corrosion cracks can be observed on Mg–OH and Mg-16 after 3 d, and the corrosion became more serious after 7 d. When the large cracks appeared on the protective layer, the corrosive ions began to corrode the matrix, raise excessive dissolution of the magnesium alloy and generate many bubbles as well as cause the rapid rise of pH value of the corrosive medium, finally leading to serious corrosion. The corrosion resistance of Mg-GOCS and Mg-GOCS/Hep was better than other samples, there was no sign of corrosion in 1d, and only small microcracks appeared in 3d. Mg-GOCS was a single-layer coating and it cannot provide long-term protection for the magnesium alloy surface. After 7 d immersion, the cracks began to expand and a small amount of corrosion products appeared on Mg-GOCS, while no large crack on the Mg-GOCS/Hep surface can be observed. As compared with that of 3 d, the number of cracks increased slightly, indicating that the increase of coating thickness could effectively improve the corrosion resistance. Therefore, the corrosion electrochemical behaviors of the magnesium alloys can be effectively controlled by changing the number and thickness of the deposited layers. In addition, it can be clearly seen that the multilayer coating can keep relative intact and compact in SBF under shaking conditions after 7 days immersion, indicating that the bonding force between coating and substrate was better.

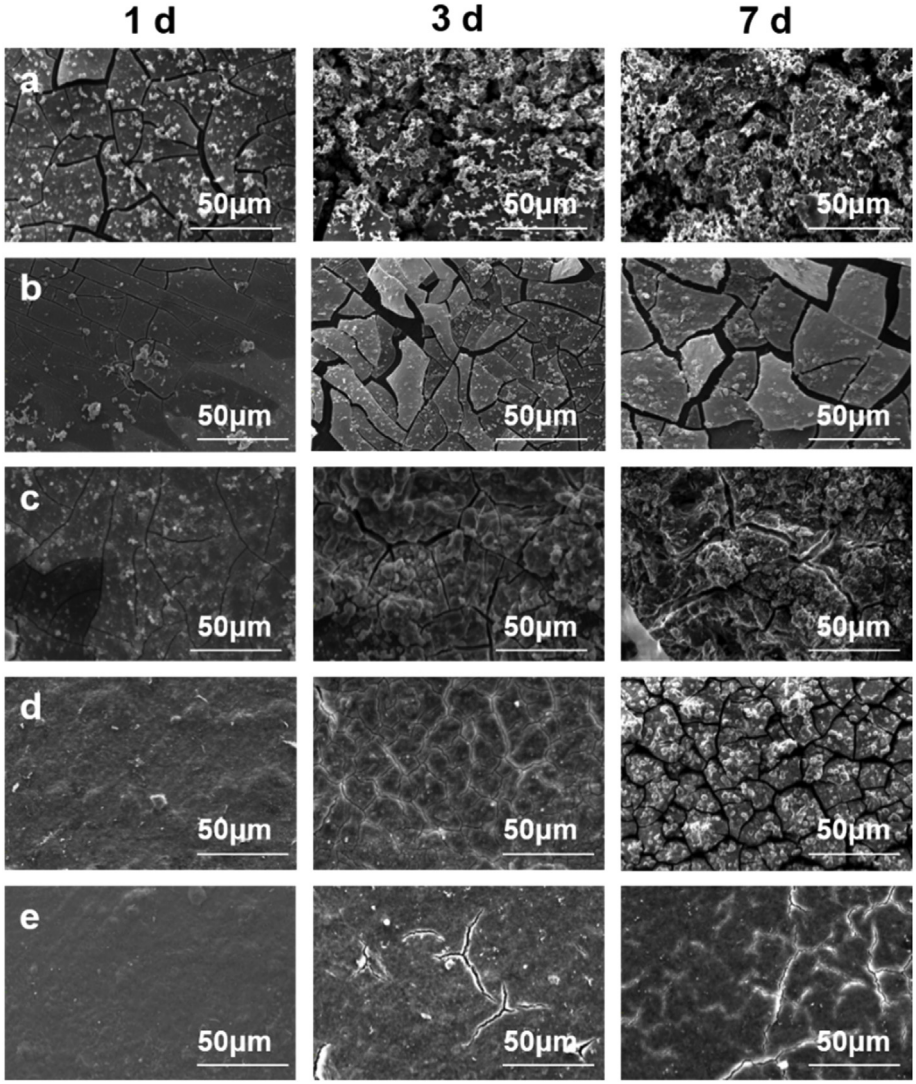

Fig. 4. Typical SEM images of the different samples immersed in SBF for 1d, 3d, and 7d. (a) Mg; (b) Mg–OH; (c) Mg-16; (d) Mg-GOCS; (e) Mg-GOCS/Hep.

In the light of the magnesium alloy corrosion mechanism, magnesium ion and hydroxide ion can be produced during the corrosion process. Therefore, the corrosion rate of the magnesium alloys can be further evaluated by the pH change of the immersion solution and the release rate of Mg^{2+} [32]. It can be seen from Fig. 5a that the pH value of all solutions increased with the increase of the immersion time. The pH value of the solution soaking the unmodified magnesium alloy was always the largest as compared to other samples, indicating that its corrosion rate was the fastest. As compared with the blank magnesium alloy, the pH values of Mg–OH and Mg-16 decreased to a certain extent due to the improved corrosion resistance by alkali heat treatment and self-assembly of 16-phosphonyl-hexadecanoic acid. The pH value of Mg-GOCS was relatively lower because GOCS can form a compact and dense modified layer on the magnesium alloy surface to slow down the corrosion rate. It was worth noting that the pH value of Mg-GOCS/Hep solution was the lowest, even after 7 d immersion, the pH value was only 8.55, indicating that the corrosion resistance was the best. As shown in Fig. 4e, there were no obvious cracks on Mg-GOCS/Hep surface after 7 d, and it still had a relatively complete covering effect on the magnesium alloy, therefore it was more beneficial to the long-term protection for the magnesium alloy surface.

In order to further evaluate the degradation behaviors, the concentration of Mg^{2+} released from the magnesium alloy was measured, and the results are shown in Fig. 5b. For the blank magnesium alloy, the Mg^{2+} release increased with the immersion time, and the value reached 32.94 μg/ml at 7d, indicating that the corrosion resistance of the unmodified magnesium alloy was poor, and it could degrade rapidly in human body. The results of the electrochemical tests showed that the

Table 4
The EIS fitting parameters of the different samples.

Samples	Rs/(Ω·cm^2)	Q_1/(μF·cm^{-2})	n_1	R_1/(Ω·cm^2)	Q_2/(μF·cm^{-2})	n_2	R_2/(Ω·cm^2)	R_p/(Ω·cm^2)
Mg	37.90	3.616×10^{-6}	0.8186	1482	–	–	–	1482
Mg–OH	37.71	3.125×10^{-6}	0.741	1882	–	–	–	1882
Mg-16	37.34	5.587×10^{-7}	0.8179	2374	–	–	–	2374
Mg-GOCS	37.15	5.008×10^{-7}	0.9167	3123	7.436×10^{-6}	0.8971	51	3174
Mg-GOCS/Hep	37.57	1.097×10^{-7}	0.8356	4257	2.357×10^{-6}	0.8438	268	4525

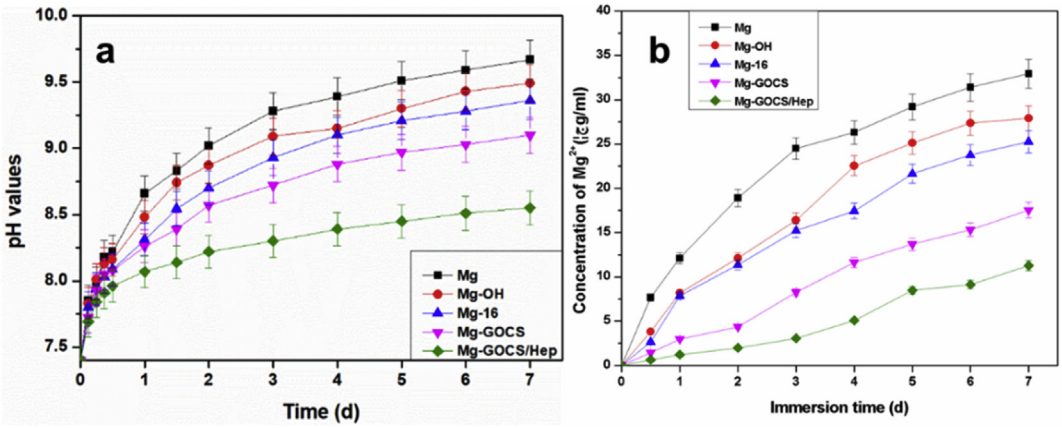

Fig. 5. (a) pH values of the immersing solutions with the different samples at the predetermined time intervals; (b) Release concentration of Mg^{2+} in the different immersing solutions.

corrosion resistance of Mg–OH and Mg-16 was improved, and the corrosion rate was slowed down after the modification, therefore the released ion concentration was decreased to some extent, but the total amount was still high, and the values were 27.91 μg/ml (Mg–OH) and 25.27 μg/ml (Mg-16) at 7 d, respectively. GOCS coating can effectively enhance the corrosion resistance of the magnesium alloy, however, the performance of the single-layer film was limited. With the extension of the immersion time, the GOCS coating could form large cracks, some of which lose the protective effect, therefore, in the early immersion stage, the release of Mg^{2+} in Mg-GOCS was less, and it started to increase rapidly at 3 d. The release of Mg^{2+} of Mg-GOCS/Hep solution was the lowest in the whole process of immersion. The Mg^{2+} content in the solution was 11.28 μg/ml at 7 d which was only about one third of the unmodified magnesium alloy, indicating that the increase of coating thickness can significantly improve the corrosion resistance.

3.3. Blood compatibility

Human blood is mainly composed of red blood cells, platelets, proteins and organic compounds. After stent implantation, it will inevitably interact with various components of blood for a long time. Materials with poor blood compatibility can cause severe hemolysis and platelet aggregation, leading to thrombus and damage to the physiological environment in blood vessels [23,33]. It was also reported that blood can trigger the corrosion of the magnesium alloy and accelerate its degradation, so that the magnesium alloy may lose its mechanical properties early in the blood vessel [34,35]. Therefore, the hemolysis rate, platelet adhesion and activation were investigated to evaluate the blood compatibility of the magnesium alloys before and after the surface modification.

Fig. 6 is the typical SEM images and the number of platelets adhered on the different surfaces. There were many platelets adhered on the unmodified magnesium alloy surface. The platelet adhesion depends on the binding of fibrinogen to the material surface, and fibrinogen is more likely to be adsorbed on the surface with poor wettability, resulting in serious platelet aggregation [36,37]. The surface hydrophobicity of the blank Mg surface was relatively high, so it can recruit more platelets on its surface and a risk of thrombus may be formed as a stent material. Alkali heat treatment can introduce a lot of hydroxyl groups on the magnesium alloy surface to improve the wettability, therefore it can effectively inhibit the fibrinogen adsorption and ultimately effectively prevent the platelet adhesion. After the immobilization of 16-phosphonyl-hexadecanoic acid, the corrosion resistance was improved obviously, and it also showed a good anti platelet adhesion. However, the number of platelets on Mg-16 surface was still about 7000 platelets/mm^2, indicating that its anticoagulant performance needed to be further improved. Chitosan can promote the adhesion and aggregation of platelets. Some studies have shown that mixing chitosan with graphene oxide had good blood compatibility [38], therefore, the number of platelets adhered on Mg-GOCS surface decreased. There was almost no platelet adhesion on the Mg-GOCS/Hep surface. On the one hand, heparin has excellent anticoagulant effect, and its anticoagulant activity is mainly caused by sulfate, sulfanilamide and carboxylic acid groups. On the other hand, the heparin coating on the magnesium alloy surface endowed the surface with excellent surface wettability, which can effectively prevent the adsorption of fibrinogen, thus significantly reduce the platelet adhesion.

Studies have shown that NO-cGMP signaling mediates and regulates many important physiological processes, including the prevention of platelet activation and aggregation. The expression of cGMP reflects the degree of platelet activation. Generally, more cGMP expression means the lower degree of platelet activation [39,40]. Fig. 7a is the cGMP expression concentration of the different sample. It was obvious that the surface modification of the magnesium alloys had obvious influence on cGMP expression. The cGMP expression concentration of the platelets on the control surface (Mg) was the lowest (only 27 nm/L), indicating that the untreated magnesium alloy had a great influence on stimulating platelet activation. As a result, compared with the modified samples, the unmodified magnesium alloy can significantly promote the platelet activation. After alkali heat treatment and the subsequent self-assembly, the cGMP expression concentration of platelets gradually increased, suggesting that the modified surface can effectively inhibit the platelet activation. The cGMP on the Mg-GOCS surface increased further, which was closely related to the anti-platelet adhesion of GOCS. It should be noted that the cGMP expression on the Mg-GOCS/Hep surface increased significantly, indicating that Mg-GOCS/Hep had a significant inhibitory effect on the platelet activation because the released heparin from the surface can increase the affinity of antithrombin III and thrombin to improve the blood compatibility, reduce protein adhesion and inhibit platelet activation [41–43].

Hemolysis rate is an important method to characterize the performance of the red blood cells. The hemolysis rate of biomaterials in contact with blood should be less than 5%. Materials with poor hemolysis rate can cause serious rupture of red blood cells, which may lead to thrombosis and the implantation failure. As shown in Fig. 7b, the hemolysis rate of the unmodified magnesium alloy was 30% and cannot meet the requirements of clinical application. As shown above, the poor corrosion resistance of the unmodified magnesium alloy can produce a large amount of hydrogen peroxide and Mg^{2+}, which can increase the pH value of the blood rapidly and promote the combination of red blood cells and Ca^{2+} in the solution, finally resulting in the rupture of red blood cells and serious hemolytic reaction [44]. The hemolysis rate of Mg–OH and Mg-16 was about 15%, it was half lower than that of Mg. It can be seen from the results of pH changes and Mg^{2+}

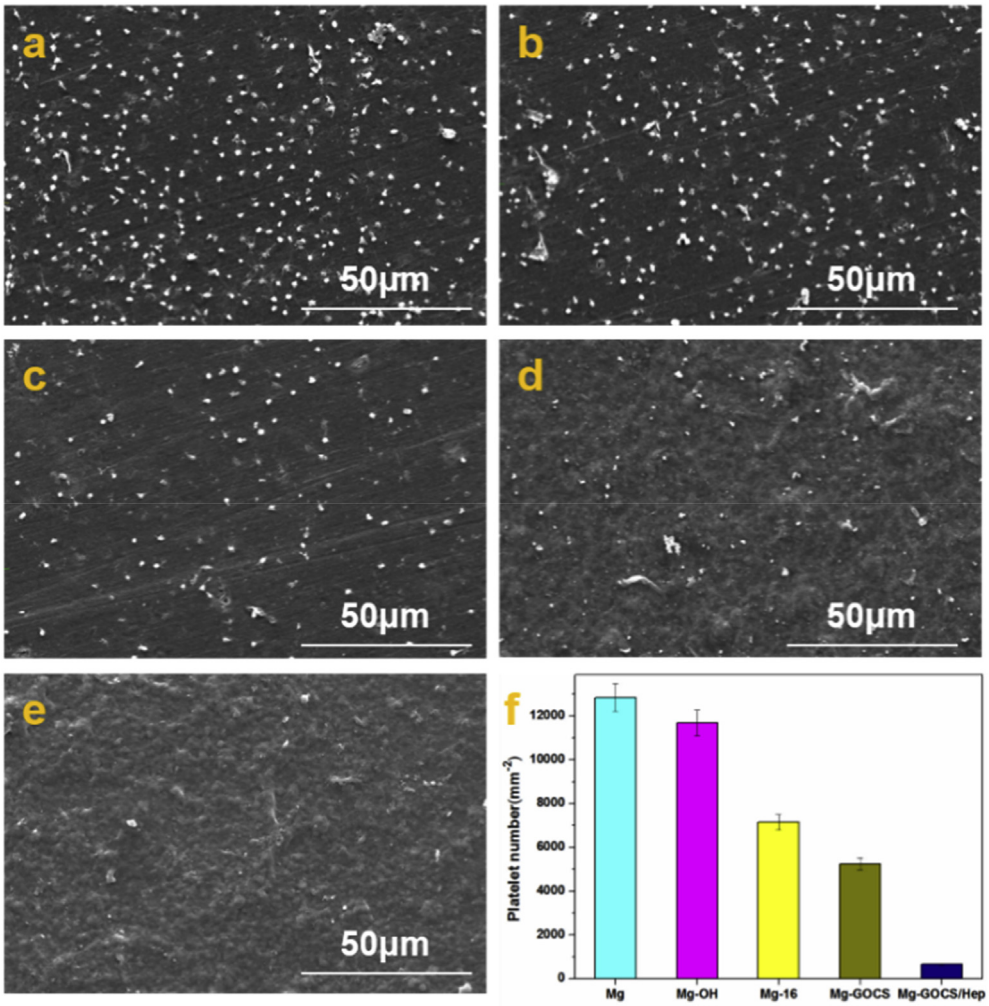

Fig. 6. The platelet adhesion quantities and typical SEM images on the different samples surfaces: (a) Mg; (b) Mg–OH; (c) Mg-16; (d) Mg-GOCS; (e) Mg-GOCS/Hep; (f) the number of platelets adhered on the different samples.

release experiments that alkali heat treatment and the surface immobilization of 16-phosphonyl-hexadecanoic acid can effectively reduce the pH changes and Mg^{2+} release, thus the damage to red blood cells was less when contacting with blood. The amino group with the positive charges on chitosan can combine with the glycoprotein with the negative charges on the surface of red blood cell membrane, causing the bending and rupture of red blood cell membrane and finally leading to the unsatisfactory blood compatibility [45]. Adding a small amount of graphene oxide to chitosan can improve the blood compatibility, because graphene oxide has a large specific surface area and the oxygen-containing negatively charged groups on the surface can reduce the impact of chitosan on red blood cells [46,47]. Consequently, the hemolysis rate of Mg-GOCS was significantly reduced, but still more than 5%. After layer by layer deposition of GOCS and heparin, a large amount of heparin was loaded on the surface and the hemolysis rate was reduced to 3%. On one hand, the better corrosion resistance can

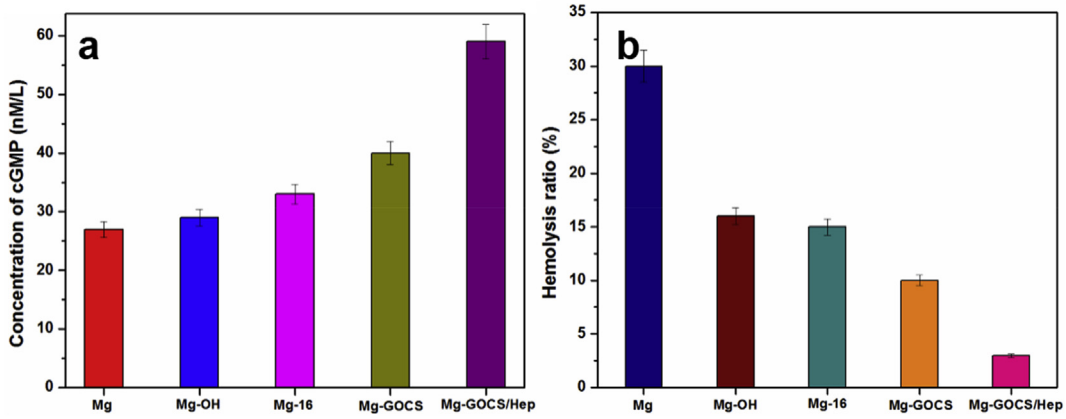

Fig. 7. (a) cGMP expression concentration (a) and hemolysis rate (b) of the different samples.

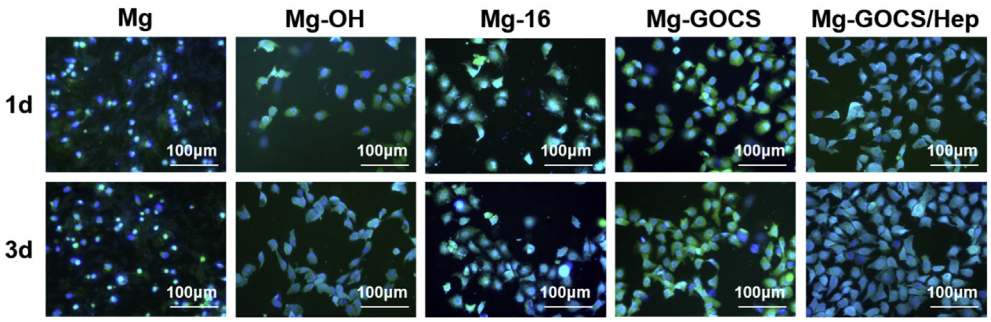

Fig. 8. Fluorescent images of the endothelial cells cultured on the different magnesium alloys for 1d and 3d (green is cytoplasm, blue is nucleus).

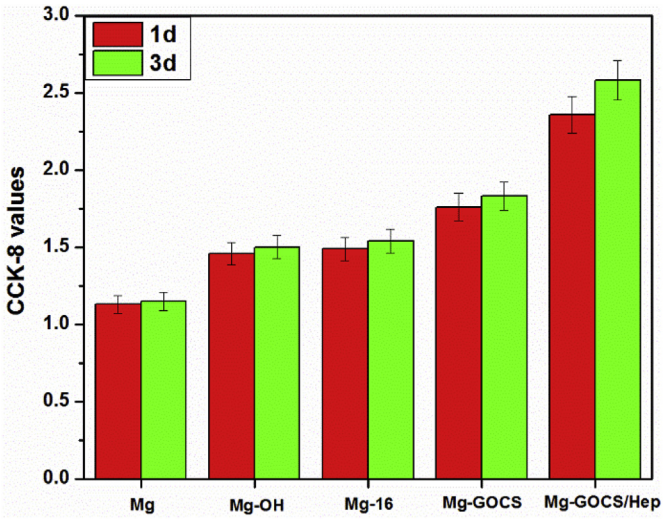

Fig. 9. The endothelial cell proliferation on different samples characterized by CCK-8 assay, the cells were cultured for 1 d and 3 d, respectively.

reduce the influence of pH values on red blood cells. On the other hand, the negatively charged carboxyl group on heparin can preferentially combine with Ca^{2+}, greatly reduce the impact of Ca^{2+} on red blood cells. In addition, heparin can be released continuously from the LBL multilayer coating, which can keep the low hemolysis rate of the magnesium alloys.

3.4. Endothelial cell behaviors

The regeneration of the healthy endothelial cell layer is very important for the success of the cardiovascular stent implantation. The purpose of stent surface modification is to build a friendly physiological microenvironment to promote endothelial cell growth and intima regeneration. Appropriate degradation rate and good biocompatibility are important prerequisites for promoting endothelial cell adhesion, proliferation and functional expression [48]. Fig. 8 shows the fluorescent images of the endothelial cells cultured on the different surfaces for 1d and 3d, respectively. Clearly, most of the cells on the blank magnesium alloy surface were shrunk and had no spreading morphologies, indicating that most of the cells may be died. It also suggested that the blank magnesium alloy cannot provide a suitable growth platform for the endothelial cells. It was concluded that the poor corrosion resistance of the pristine magnesium alloy could made it difficult for cell adhesion and growth in the human environment, and the bubbles and high pH value in the surrounding environment caused by the fast corrosion were not beneficial to the attachment and growth of endothelial cells. At the same time, magnesium alloy surface had no bioactivities and cell receptors, and therefore it counted against the cell recruitment. There were more endothelial cells on Mg–OH and Mg-16 surfaces, and the number of cells cultured for 3 d was significantly more than that of cultured for 1 d, indicating that the endothelial cells can grow on the modified magnesium alloy surface. It was considered that the improved corrosion resistance after the preliminary treatment can reduce the impact of corrosion on the cytotoxicity of the magnesium alloys. Some studies have shown that graphene oxide can promote the ECM protein adsorption through noncovalent interaction, electrostatic forces or hydrogen bonds, thus leading to better cell adhesion and growth [49,50]. In addition, chitosan has good biocompatibility and it can significantly promote the migration and proliferation of the vascular endothelial cells [51]. Therefore, the number of the endothelial cells on Mg-GOCS increased significantly with better spreading morphologies. The cell adhesion and proliferation on the Mg-GOCS/Hep surface was the best, and the surface was almost covered by cells at 3 d. On one hand, the improved corrosion resistance of the GOCS/Hep multilayer can effectively reduce the influences of corrosion on endothelial cells. On the other side, the good surface wettability of the bioactive GOCS/Hep multilayer was beneficial to the ECM adsorption, which was contributed to the endothelial cells adhesion and spreading.

CCK-8 reagent is widely used to detect cell proliferation. It contains WST-8 that can be reduced by dehydrogenase in the cell to a highly water-soluble yellow methylazan product, which is proportional to the number of living cells, consequently the cell proliferation can be analyzed by CCK-8 assay [52]. Fig. 9 shows the CCK-8 values of the different samples. There was almost no difference for the CCK- 8 values of the Mg surface between 1 d and 3 d, suggesting that with the increase of culture time, the endothelial cells did not differentiate and proliferate on the pristine Mg surface. The results of cell adhesion suggested that most of the endothelial cells on the blank Mg surface exhibited apoptosis, which may have no proliferation ability and thus had the lowest CCK-8 values. The CCK-8 values on NaOH-treated and Mg-16 surfaces had no obvious difference, but their values were significantly higher than that of Mg, and the CCK- 8 value of 3d was higher than that of 1d, which can be attributed to the decrease of pH value resulting from the improved corrosion resistance after the surface modification. The CCK-8 value of the cells on the Mg-GOCS surface further increased, indicating that there were many living cells on the surface. Because GOCS can not only significantly improve the corrosion resistance of the magnesium alloy, but also enhance the surface bioactivities, and consequently the immobilization of GOCS can promote the proliferation of the endothelial cells. In particular, the CCK-8 value for the Mg-GOCS/Hep surface increased significantly as compared to other samples, and the value (2.58) in 3d was above twice than that of the unmodified magnesium alloy, suggesting that the endothelial cells can proliferate well because the introduction of GOCS and heparin on the surface can not only reduce the effect of cytotoxicity caused by the corrosion but also improve the growth of the endothelial cells. As a result, the GOCS/Hep multilayer coating can provide a good environment for the endothelial cell adhesion and proliferation.

VEGF is a highly specific vascular endothelial growth factor and it can induce the expression of plasma plasminogen activator and

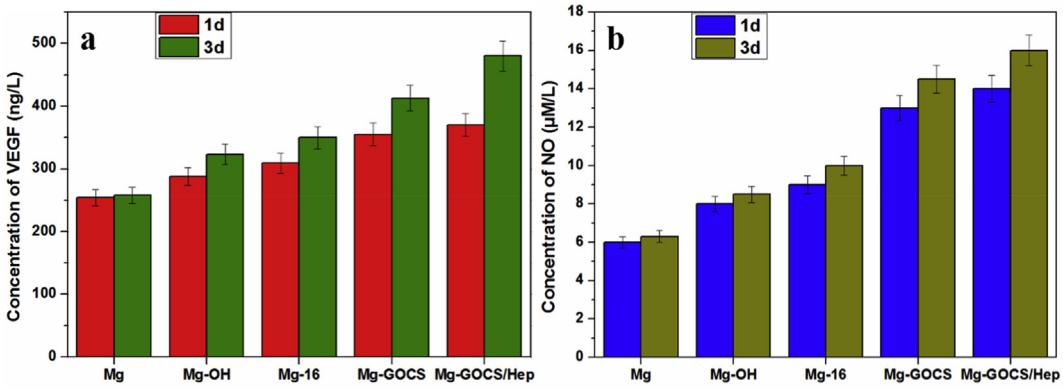

Fig. 10. VEGF (a) and NO (b) release for the different samples.

plasminogen activator inhibitor-1, as well as matrix collagenase and other factors in endothelial cells. It also can stimulate the release of V3 factor from the endothelial cells, thereby changing the extracellular matrix and promoting the growth of the vascular endothelial cells [53]. Normal endothelial cells can express a certain amount of VEGF, and its expression can further promote the growth of the endothelial cells, therefore it is important to explore the VEGF expression to investigate the effect of the implanted vascular stent on the functions of endothelial cells. Fig. 10a shows the results of the VEGF concentration for the different samples. Even though the cells adhered on Mg surface was less, it also maintained a certain amount of VEGF concentration (258 ng/L), however, the value was the lowest among all samples. NaOH treatment and the immobilization of 16-phosphonyl-hexadecanoic acid on the surface increased the expression concentration of VEGF to some degree, which can be due to the improvement of the corrosion resistance. A higher VEGF concentration can maintain endothelial function and promote endothelial cell differentiation [54]. The concentration of VEGF for Mg-GOCS and Mg-GOCS/Hep increased significantly (Mg-GOCS, 387 ng/L; Mg-GOCS/Hep, 430 ng/L), indicating that the good biological activities of GOCS and heparin could effectively maintain the expression of VEGF in endothelial cells. It was worth noting that on the multilayer surface, the VEGF expression concentration of the endothelial cells was the highest. On one hand, the improved corrosion resistance by layer-by-layer deposition of the bioactive substances can contribute to keep normal functional expression of endothelial cells. On the other hand, in addition to good blood compatibility, heparin also has an obvious effect on promoting VEGF expression of endothelial cells, which is conducive to promoting endothelial cell proliferation and inducing angiogenesis [55].

NO is a signal molecule produced when endothelial cells synthesize and secrete, which plays an important role in several physiological processes, including anti-atherosclerosis, stimulation of endothelial cell growth and vasodilation, and inhibition of the platelet adhesion [56,57]. In various animal models, NO release on the modified surface can effectively improve the effect of antithrombotic and anti-restenosis [58,59]. In the present study, the nitrate reductase method was used to study the NO expression of the endothelial cells on the surfaces, and the results are shown in Fig. 10b. Clearly, a significant difference in the concentration of NO expression for the different magnesium alloy surfaces can be found. In general, the healthy vascular endothelium in human body has NO expression. The damage of the natural endothelium could lead to the loss of the endothelial function and thus reduce the amount of NO synthesis. The rapid corrosion rate of Mg caused serious damage to endothelial cells and limited the functional expression of endothelial cells, therefore the concentration of NO released by the endothelial cells was low. The better corrosion resistance can reduce the effect of excessive corrosion on cells, and the self-assembly modification can significantly improve the corrosion resistance, therefore it can promote the release of NO from endothelial cells to a certain extent. However, the bioactivities of Mg–OH and Mg-16 were limited and thus they showed a limited ability to promote cell growth and NO expression. In contrast, the surfaces of Mg-GOCS and Mg-GOCS/Hep can significantly promote the NO expression, which was of great significance to improve the biocompatibility of the magnesium alloys. This was because NO is an important indicator of maintaining the normal physiological function of the endothelial cells. NO can cooperate with heparin, which can not only stimulate the growth of the endothelial cells, but also increase the concentration of cGMP in platelets, reduce the level of intracellular Ca^{2+}, and thus prevent the adhesion and activation of platelets and fibrinogen [48,60]. This was not only related to the excellent corrosion resistance and biological activity of GOCS/Hep multilayer coating, but also due to its ability to promote NO release.

Taking all above results into consideration, it can be concluded that the GOCS/Hep bioactive multilayer coating can not only significantly improve the corrosion resistance of the magnesium alloy, but also obviously enhance the blood compatibility and promote the growth of the endothelial cells. The mechanism of the coating on the corrosion resistance and biocompatibility can be explained as shown in Fig. 11. Before the surface modification, the magnesium alloy has poor corrosion resistance and limited biological activities. Cl^- is easy to erode the matrix surface, resulting in the surface corrosion defects and serious corrosion. The released hydrogen and magnesium ions can form serious hemolytic reaction and cause platelet adhesion and activation. At the same time, the hydrogen bubbles and surface defects caused by the fast corrosion also strongly inhibit the adhesion and growth of the endothelial cells. After layer by layer deposition of GOCS and heparin, the thicker coating and the outermost heparin with the negative charges can effectively inhibit the corrosion of Cl^- on the magnesium alloy and reduce the impact of excessive corrosion on cells and blood. In the meantime, the continuous release of heparin endows the material with good blood compatibility, which can significantly reduce the hemolysis rate, platelet adhesion and activation. In addition, the improvement of the corrosion resistance effectively inhibits the degradation of the magnesium alloy, and significantly reduces the release of magnesium ion and OH^-. Both GOCS and heparin can promote the growth of the endothelial cells. These factors can effectively promote the growth of the endothelial cells and the functional expression of NO and VEGF. The increase of VEGF is beneficial to the growth of the endothelial cells and the formation of vascular endothelial layer. NO and heparin work together to further inhibit platelet activation and promote the growth of the endothelial cells.

4. Conclusion

In this paper, the positively charged GOCS and negatively charged heparin were alternatively deposited on the magnesium alloy surface by the LBL to construct the GOCS/Hep bioactive multilayer coating. The

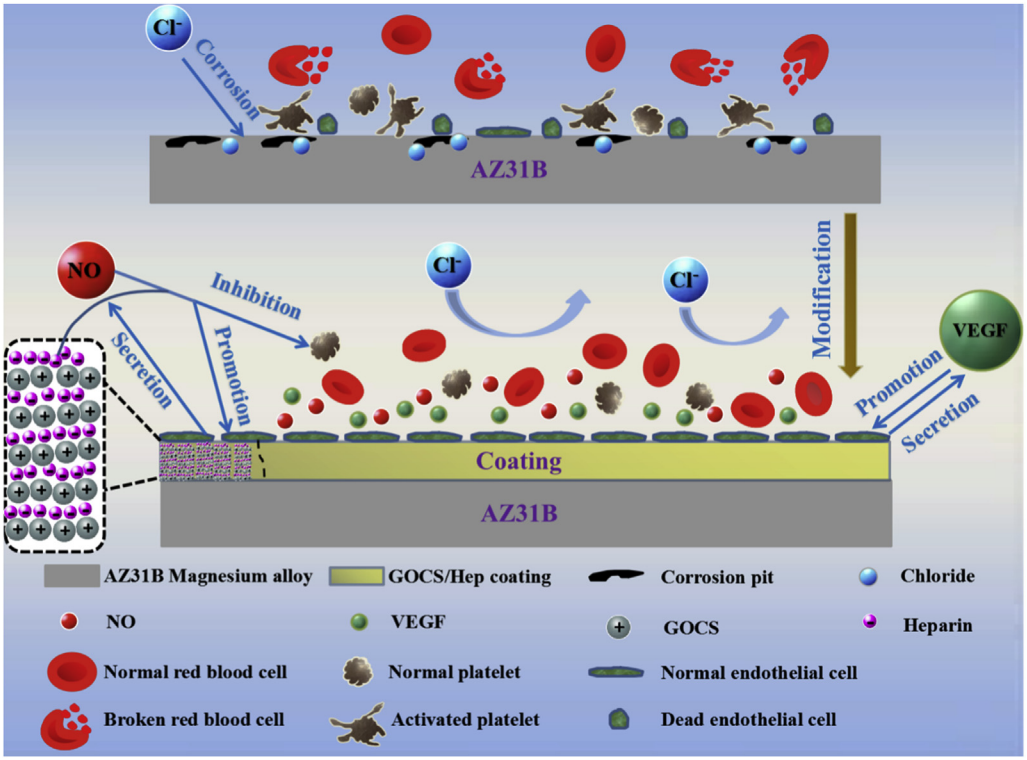

Fig. 11. Mechanism of GOCS/Hep multilayer coating on the corrosion resistance and biocompatibility of the magnesium alloy surface.

corrosion and biocompatibility were in detail investigated and the conclusions were as follows.

(1) The corrosion resistance of magnesium alloy was significantly improved by GOCS/Hep multilayers. Due to the dense and thicker coating and the inhibition of anion adsorption of the negatively charged heparin, the degradation of the magnesium alloy in the corrosive solution was reduced obviously, and the impact on the pH value of the surrounding environment was small.
(2) The GOCS/Hep multilayer coating had good blood compatibility, it can not only significantly reduce the hemolysis rate of magnesium alloy, but also inhibit platelet adhesion and activation. At the same time, the multilayer coating can enhance the adhesion and proliferation of the endothelial cells and significantly promote the NO and VEGF expression.
(3) In conclusion, the GOCS/Hep multilayer coating can not only improve the corrosion resistance of magnesium alloy, but also simultaneously enhance the blood compatibility and endothelial proliferation, which is expected to solve the problems of the rapid degradation and the limited biocompatibility of the magnesium alloy stent materials.

CRediT authorship contribution statement

Fan Gao: Methodology, Investigation, Writing - original draft. **Youdong Hu:** Investigation, Writing - original draft. **Guicai Li:** Methodology, Validation. **Sen Liu:** Formal analysis. **Li Quan:** Data curation. **Zhongmei Yang:** Writing - review & editing. **Yanchun Wei:** Writing - review & editing. **Changjiang Pan:** Conceptualization, Resources, Supervision, Writing - review & editing.

Declaration of competing interest

The authors declare that they have no known competing financial interests or personal relationships that could have appeared to influence the work reported in this paper.

Acknowledgements

This work is financially supported by the National Natural Science Foundation of China (31870952), Natural Science Foundation of Jiangsu Province of China (BK20181480), The Key Program of National Natural Science Foundation of China (31830028), the International S& T Cooperation Program of Huai'an City of China (HAC201703), and the Key Program for Natural Science Foundation of Jiangsu Higher Education Institutions of China (17KJA530002).

References

[1] E. Im, S.Y. Lee, S.J. Hong, C.M. Ahn, J.S. Kim, B.K. Kim, Y.G. Ko, D. Choi, Y. Jang, M.K. Hong, Impact of late stent malapposition after drug-eluting stent implantation on long-term clinical outcomes, Atherosclerosis 288 (2019) 118–123.
[2] Y.J. Shi, J. Pei, L. Zhang, B.K. Lee, Y. Yun, J. Zhang, Z.H. Li, S. Gu, K. Park, G.Y. Yuan, Understanding the effect of magnesium degradation on drug release and anti-proliferation on smooth muscle cells for magnesium-based drug eluting stents, Corrosion Sci. 123 (2017) 297–309.
[3] S. Ramcharitar, P.W. Serruys, Fully biodegradable coronary stents: progress to date, Am. J. Cardiovasc. Drugs 8 (2008) 305–314.
[4] H. Jodati, B. Güner, Z. Evis, D. Keskin, A. Tezcaner, Synthesis and characterization of magnesium-lanthanum dual doped bioactive glasses, Ceram. Int. 46 (2020) 10503–10511.
[5] Y.Z. Wan, G.Y. Xiong, H.L. Luo, F. He, Y. Huang, X.S. Zhou, Preparation and characterization of a new biomedical magnesium-calcium alloy, Mater. Des. 29 (2008) 2034–2037.
[6] J. Liao, M. Hotta, K. Kaneko, K. Kondoh, Enhanced impact toughness of magnesium alloy by grain refinement, Scripta Mater. 61 (2009) 208–211.
[7] Y.Y. Yin, W.C. Qi, R.C. Zeng, X.B. Chen, C.D. Gu, S.K. Guan, Y.F. Zheng, Advances in coatings on biodegradable magnesium alloys, J. Magnesium Alloys 8 (2020) 42–65.
[8] L.Y. Li, L.Y. Cui, R.C. Zeng, S.Q. Li, X.B. Chen, Y.F. Zheng, M.B. Kannan, Advances in functionalized polymer coatings on biodegradable magnesium alloys-A review, Acta Biomater. 9 (2018) 23–36.
[9] J.F. Song, J. She, D.L. Chen, F.S. Pan, Latest research advances on magnesium and magnesium alloys worldwide, J. Magnesium Alloys. 8 (2020) 1–41.
[10] M.S. Song, R.C. Zeng, Y.F. Ding, R.W. Li, M. Easton, I. Cole, N. Birbilis, X.B. Chen, Recent advances in biodegradation controls over Mg alloys for bone fracture management: a review, J. Mater. Sci. Technol. 35 (2019) 535–544.
[11] Z.Q. Shen, M. Zhao, D. Bian, D.N. Shen, X.C. Zhou, J.N. Liu, Y. Liu, H. Guo,

Y.F. Zheng, Predicting the degradation behavior of magnesium alloys with a diffusion-based theoretical model and in vitro corrosion testing, J. Mater. Sci. Technol. 35 (2019) 1393–1402.
[12] Y.C. Ozaki, M.G.G. Hector, S. Evan, H.K. Alexandre, W. Ron, Second-generation drug-eluting resorbable magnesium scaffold: review of the clinical evidence, Cardiovasc. Revascularization Med. 21 (2020) 127–136.
[13] W. Yan, Y.J. Lian, Z.Y. Zhang, M.Q. Zeng, Z.Q. Zhang, Z.Z. Yin, L.Y. Cui, R.C. Zeng, *In vitro* degradation of pure magnesium—the synergetic influences of glucose and albumin, Bioact. Mater. 5 (2020) 318–333.
[14] Y.X. Yang, Z. Fang, Y.H. Liu, Y.C. Hou, L.G. Wang, Y.F. Zhou, S.J. Zhu, R.C. Zeng, Y.F. Zheng, S.K. Guan, Biodegradation, hemocompatibility and covalent bonding mechanism of electrografting polyethylacrylate coating on Mg alloy for cardiovascular stent, J. Mater. Sci. Technol. 46 (2020) 114–126.
[15] Y.B. Zhao, L.Q. Shi, X.J. Ji, J.C. Li, Z.Z. Han, S.Q. Li, R.C. Zeng, F. Zhang, Z.L. Wang, Corrosion resistance and antibacterial properties of polysiloxane modified layer-by-layer assembled self-healing coating on magnesium alloy, J. Colloid Interface Sci. 526 (2018) 43–50.
[16] *In vitro* corrosion resistance of layer-by-layer assembled polyacrylic acid multilayers induced Ca-P coating on magnesium alloy AZ31, Bioact. Mater. 5 (2020) 153–163.
[17] H.R. Bakhsheshi-Rad, E. Hamzah, M. Kasiri-Asgarani, S.N. Saud, F. Yaghoubidoust, E. Akbari, Structure, corrosion behavior, and antibacterial properties of nano-silica/graphene oxide coating on biodegradable magnesium alloy for biomedical applications, Vacuum 131 (2016) 106–110.
[18] Y. Luo, H. Shen, Y. Fang, Y. Cao, J. Huang, M. Zhang, J. Dai, X. Shi, Z. Zhang, Enhanced proliferation and osteogenic differentiation of mesenchymal stem cells on graphene oxide-incorporated electrospun poly(lactic-co-glycolic acid) nanofibrous mats, ACS Appl. Mater. Interfaces 7 (2015) 6331–6339.
[19] N. Erika, M. Hirofumi, K. Akihito, T. Hiroko, I. Toshihiko, M. Takehito, O. Kosuke, M. Shusuke, S. Tsutomu, K. Masamitsu, Graphene oxide scaffold accelerates cellular proliferative response and alveolar bone healing of tooth extraction socket, Int. J. Nanomed. 11 (2016) 2265–2277.
[20] H. Xu, Y.W. Ge, J.W. Lu, Q.F. Ke, Z.Q. Liu, Z.A. Zhu, Y.P. Guo, Icariin loaded-hollow bioglass/chitosan therapeutic scaffolds promote osteogenic differentiation and bone regeneration, Chem. Eng. J. 354 (2018) 285–294.
[21] X.N. Gu, Y.F. Zheng, Q.X. Lan, Y. Cheng, Z.X. Zhang, T.F. Xi, D.Y. Zhang, Surface modification of an Mg-1Ca alloy to slow down its biocorrosion by chitosan, Biomed. Mater. 4 (2009) 044109.
[22] E. Young, The anti-inflammatory effects of heparin and related compounds, Thromb. Res. 122 (2008) 743–752.
[23] C.J. Pan, Y.H. Hou, B.B. Zhang, et al., Blood compatibility and interaction with endothelial cells of titanium modified by sequential immobilization of poly (ethylene glycol) and heparin, J. Mater. Chem. B. 2 (2014) 892–902.
[24] C.Y. Ho, S.M. Huang, S.T. Lee, Y.J. Chang, Evaluation of synthesized graphene oxide as corrosion protection film coating on steel substrate by electrophoretic deposition, Appl. Surf. Sci. 477 (2019) 226–231.
[25] X.F. Zhai, K. Li, F. Guan, C.T. Sun, J.Z. Duan, B.R. Hou, Corrosion behavior of the chitosan-zinc composite films in sulfate-reducing bacteria, Surf. Coating. Technol. 344 (2018) 259–268.
[26] M. Zhou, L.C. Yan, H. Ling, Y.P. Diao, X.L. Pang, Y.L. Wang, K.W. Gao, Design and fabrication of enhanced corrosion resistance Zn-Al layered double hydroxides films based anion-exchange mechanism on magnesium alloys, Appl. Surf. Sci. 404 (2017) 246–253.
[27] C.J. Pan, Y. Hou, Y.N. Wang, F. Gao, T. Liu, Y.H. Hou, Y.F. Zhu, W. Ye, L.R. Wang, Effects of self-assembly of 3-phosphonopropionic acid, 3-aminopropyltrimethoxysilane and dopamine on the corrosion behaviors and biocompatibility of a magnesium alloy, Mater. Sci. Eng. C 67 (2016) 132–143.
[28] V. Berry, Impermeability of graphene and its applications, Carbon 62 (2013) 1–10.
[29] B.Y. Chang, S. M Park, Electrochemical impedance spectroscopy, Annu. Rev. Anal. Chem. 3 (2010) 207–229.
[30] F. Zanotto, V. Grassi, A. Frignani, F. Zucchi, Protection of the AZ31 magnesium alloy with cerium modified silane coatings, Mater. Chem. Phys. 129 (2011) 1–8.
[31] P. Chakraborty Banerjee, R.K. Singh Raman, Electrochemical impedance spectroscopic investigation of the role of alkaline pre-treatment in corrosion resistance of a silane coating on magnesium alloy, ZE41, Electrochim. Acta 56 (2011) 3790–3798.
[32] C.J. Pan, Y.D. Hu, Y. Hou, T. Liu, Y.B. Lin, W. Ye, Y.H. Hou, T. Gong, Corrosion resistance and biocompatibility of magnesium alloy modified by alkali heating treatment followed by the immobilization of poly (ethylene glycol), fibronectin and heparin, Mater. Sci. Eng. C 70 (2017) 438–449.
[33] K.N. Sask, W.G. McClung, L.R. Berry, A.K.C. Chan, J. L Brash, Immobilization of an antithrombin-heparin complex on gold: anticoagulation properties and platelet interactions, Acta Biomater. 7 (2011) 2029–2034.
[34] J. Geis-Gerstorfer, C. Schille, E. Schweizer, F. Rupp, I. Scheideler, H.P. Reichel, J. Hort, A. Nolte, H.P. Wendel, Blood triggered corrosion of magnesium alloy, Mater. Sci. Eng. B 176 (2011) 1761–1766.
[35] C. Schille, M. Braun, H.P. Wendel, L. Scheideler, N. Hort, H.P. Reichel, E. Schweizer, J. Geis-Gerstorfer, Corrosion of experimental magnesium alloys in blood and PBS, a gravimetric and microscopic evaluation, Mater. Sci. Eng. B. 176 (2011) 1797–1801.
[36] W.B. Tsai, J.M. Grunkemeier, C.D. McFarland, T.A. Horbett, Platelet adhesion to polystyrene-based surfaces pre-adsorbed with plasmas selectively depleted in fibrinogen, fibronectin, vitronectin, or von Willebrand's factor, J. Biomed. Mater. Res. 60 (2002) 348–359.
[37] L. D Zhang, B. Casey, D.K. Galanakis, C. Marmorat, S. Skoog, K. Vorvolakos, M. Simon, M.H. Rafailovich, The influence of surface chemistry on adsorbed fibrinogen conformation, orientation, fiber formation and platelet adhesion, Acta Biomater. 54 (2017) 164–174.
[38] K.H. Liao, Y.S. Lin, C.W. MacOsko, C.L. Haynes, Cytotoxicity of graphene oxide and graphene in human erythrocytes and skin fibroblasts, ACS Appl. Mater. Interfaces 3 (2011) 2607–2615.
[39] Z.L. Yang, Y. Yang, K.Q. Xiong, X.Y. Li, P.K. Qi, Q.F. Tu, F.J. Jing, Y.J. Weng, J. Wang, N. Huang, Nitric oxide producing coating mimicking endothelium function for multifunctional vascular stents, Biomaterials 63 (2015) 80–92.
[40] O. Ros, Y. Zagar, S. Ribes, S. Baudet, K. Loulier, S. Couvet, D. Ladarre, A. Aghaie, A. Louail, C. Petit, Y. Mechulam, Z. Lenkei, X. Nicol, SponGee: a genetic tool for subcellular and cell-specific cGMP manipulation, Cell Rep. 27 (2019) 4003–4012.
[41] F. Gong, X. Cheng, S. Wang, Y. Zhao, Y. Gao, H. Cai, Heparin-immobilized polymers as non-inflammatory and non-thrombogenic coating materials for arsenic trioxide eluting stents, Acta Biomater. 6 (2010) 534–546.
[42] Z. Yang, J. Wang, R. Luo, M.F. Maitz, F. Jing, H. Sun, N. Huang, The covalent immobilization of heparin to pulsed-plasma polymeric allylamine films on 316L stainless steel and the resulting effects on hemocompatibility, Biomaterials 31 (2010) 2072–2083.
[43] F.R. Gong, X.Y. Cheng, S.F. Wang, Y.C. Zhao, Y. Gao, H.B. Cai, Heparin-immobilized polymers as non-inflammatory and non-thrombogenic coating materials for arsenic trioxide eluting stents, Acta Biomater. 6 (2010) 534–546.
[44] H. Zhang, L. Xie, X. Shen, T. Shang, R. Luo, X. Li, T. You, J. Wang, N. Huang, Y. Wang, Catechol/polyethyleneimine conversion coating with enhanced corrosion protection of magnesium alloys: potential applications for vascular implants, J. Mater. Chem. B. 6 (2018) 6936–6949.
[45] I.K. Kang, O.H. Kwon, Y.M. Lee, K.S. Yong, Preparation and surface characterization of functional group-grafted and heparin-immobilized polyurethanes by plasma glow discharge, Biomaterials 17 (1996) 841–847.
[46] K.K. Wu, X.Y. Liu, Z.T. Li, Y.P. Jiao, C.R. Zhou, Fabrication of chitosan/graphene oxide composite aerogel microspheres with high bilirubin removal performance, Mater. Sci. Eng. C 106 (2020) 110162.
[47] B. Cai, K.B. Hu, C.M. Li, J. Jin, Y.X. Hu, Bovine serum albumin bioconjugated graphene oxide: red blood cell adhesion and hemolysis studied by QCM-D, Appl. Surf. Sci. 356 (2015) 844–851.
[48] H. Qiu, P.K. Qi, J.X. Liu, Y. Yang, X. Tan, Y. Xiao, M.F. Maitz, N. Huang, Z.L. Yang, Biomimetic engineering endothelium-like coating on cardiovascular stent through heparin and nitric oxide-generating compound synergistic modification strategy, Biomaterials 207 (2019) 10–22.
[49] H.Q. Chen, M.B. Müller, K.J. Gilmore, G.G. Wallace, D. Li, Mechanically strong, electrically conductive, and biocompatible graphene paper, Adv. Mater. 20 (2008) 3557–3561.
[50] Y. Mei, S. Gerecht, M. Taylor, A.J. Urquhart, S.R. Bogatyrev, S.W. Cho, M.C. Davies, M.R. Alexander, R.S. Langer, D.G. Anderson, Mapping the interactions among biomaterials, adsorbed proteins, and human embryonic stem cells, Adv. Mater. 21 (2009) 2781–2786.
[51] E. Khor, L.Y. Lim, Implantable applications of chitin and chitosan, Biomaterials 24 (2003) 2339–2349.
[52] F. Gao, Y.D. Hu, Z. H Gong, T. Liu, T. Gong, S. Liu, C. Zhang, L. Quan, B. Kaveendran, C.J. Pan, Fabrication of chitosan/heparinized graphene oxide multilayer coating to improve corrosion resistance and biocompatibility of magnesium alloys, Mater. Sci. Eng. C 104 (2019) 109947.
[53] B. Wang, Y. Huang, Z.W. Huang, H. Wang, J.T. Chen, X. Pan, C.B. Wu, Self-assembling in situ gel based on lyotropic liquid crystals containing VEGF for tissue regeneration, Acta Biomater. 99 (2019) 84–99.
[54] G. Liu, L. Li, D. Huo, Y. Li, Y. Wu, L. Zeng, P. Cheng, M. Xing, W. Zeng, C. Zhu, A VEGF delivery system targeting MI improves angiogenesis and cardiac function based on the tropism of MSCs and layer-by-layer self-assembly, Biomaterials 127 (2017) 117–131.
[55] Z. Yang, Q. Tu, J. Wang, N. Huang, The role of heparin binding surfaces in the direction of endothelial and smooth muscle cell fate and re-endothelialization, Biomaterials 33 (2012) 6615–6625.
[56] A.W. Carpenter, M.H. Schoenfisch, Nitric oxide release: Part II. Therapeutic applications, Chem. Soc. Rev. 41 (2012) 3742–3752.
[57] A.D. Mel, F. Murad, A.M. Seifalian, Nitric oxide: a guardian for vascular grafts, Chem. Rev. 111 (2011) 5742–5767.
[58] M.C. Jen, M.C. Serrano, R. Van Lith, G.A. Ameer, Polymer-based nitric oxide therapies: recent insights for biomedical applications, Adv. Funct. Mater. 22 (2012) 239–260.
[59] A.B. Seabra, G.Z. Justo, P.S. Haddad, State of the art, challenges and perspectives in the design of nitric oxide-releasing polymeric nanomaterials for biomedical applications, Biotechnol. Adv. 33 (2015) 1370–1379.
[60] D.J. Suchyta, H. Handa, M.E. Meyerhoff, A nitric oxide-releasing heparin conjugate for delivery of a combined antiplatelet/anticoagulant agent, Mol. Pharm. 11 (2014) 645–650.